Polarized laser selective excitation and Zeeman infrared absorption of C_{4v} and C_{3v} symmetry centers in Eu^{3+}-doped CaF_2, SrF_2, and BaF_2 crystals

Jon-Paul R. Wells* and Roger J. Reeves
Department of Physics and Astronomy, University of Canterbury, PB4800, Christchurch, New Zealand
(Received 30 January 2001; published 25 June 2001)

Laser selective excitation and Zeeman infrared-absorption spectroscopy have been employed to study Eu^{3+} centers in CaF_2, SrF_2, and BaF_2 crystals. At low dopant concentrations ($\leqslant$0.1 mol%), the dominant center for both CaF_2 and SrF_2 crystals is the well-established $C_{4v}(F^-)$ center that consists of a Eu^{3+}-F^- dipole oriented along the [100] crystallographic directions. The dominant center for BaF_2:Eu^{3+} and a second center in SrF_2:Eu^{3+} has C_{3v} symmetry with the charge compensating F^- ion residing in an interstitial position along the [111] directions. In all three crystals, nonlocally charge-compensated cubic symmetry centers are also present. Zeeman measurements of the infrared absorption transitions to the Eu^{3+} $^7F_6$ multiplet reveal interesting nonlinear Zeeman splittings as a function of the applied magnetic field. Crystal-and magnetic-field analyses of the $C_{4v}(F^-)$ and $C_{3v}(F^-)$ centers give crystal-field parameters that are in agreement with those of other rare-earth ions and that well account for the measured Zeeman splittings.

DOI: 10.1103/PhysRevB.64.035102 PACS number(s): 71.70.Ch, 71.70.Ej, 78.30.−j

I. INTRODUCTION

The alkaline-earth fluoride lattice consists of a body-centered (fluorite) cubic structure. The F^- ions form a cubic cage with the alkaline-earth cation residing at the center of each alternate cage. Trivalent rare-earth ions (R^{3+}) can be substituted for the divalent alkaline-earth cation. Some form of charge compensation is required that normally takes the form of interstitial fluorine ions. For CaF_2:R^{3+} crystals with R^{3+} concentrations less than 0.1 mol percent, the well-established $C_{4v}(F^-)$ center is predominant. This center consists of a R^{3+}-F^- pair with the charge-compensating fluorine ion located in the nearest-neighbor position along the [100] directions from the rare-earth ion.[1–9] For SrF_2:R^{3+} the center distributions are more complicated with ions in the rare-earth series up to Dy^{3+} having a predominant $C_{4v}(F^-)$ center, with a change over between Ho^{3+} and Er^3 to a center of C_{3v} symmetry.[6,10] This center consists of a R^{3+}-F^- pair with the F^- ion located in the next-nearest-neighbor position along the [111] directions from the R^{3+} ion.

The spectra of trivalent europium have received much attention in the literature.[11–19] A particular feature prompting many studies is the extreme sharpness of the $^7F_0 \rightarrow {}^5D_0$ transition for some crystalline hosts at low temperatures.[20] The width of this transition (with the implied slow optical dephasing of the excited $^5D_0$ state) is a very effective and sensitive probe of disorder created by the introduction of defects and strains during crystal growth. For CaF_2:Eu^{3+}, Voronko, Kamnskii, and Osiko used the concentration series method to obtain information on the defect distribution, inferring the presence of at least three distinct centers.[21] Zakharchenya and Rusanov[22] did optical Zeeman spectroscopy on the magnetic dipole allowed $^7F_0 \rightarrow {}^5D_1$ transitions that identified a cubic symmetry center.

With laser selective excitation, more detailed studies were undertaken. Hamers, Wietfeldt, and Wright[4] investigated the defect equilibria of CaF_2:Eu^{3+}. Five major centers were identified and these comprised a cubic O_h, tetragonal C_{4v}, a single-ion center (labeled *P*), and two-cluster centers (labeled *R* and *Q*) assigned as dimers. More recent investigations by Cirillo-Penn and Wright[23–25] have shown these centers to be the (2Eu·3F) ''*R*'' dimer and the (3Eu·4F ''*Q*'' trimer, respectively. Related Sm^{3+} centers have been observed for CaF_2:Sm^{3+} crystals[9] and mixed heterogeneous Eu^{3+}-Sm^{3+} analogues in double-doped CaF_2:Eu^{3+}:Sm^{3+} show complete energy transfer from the $^4G_{5/2}(Sm^{3+})$ multiplet to the $^5D_0(Eu^{3+})$ multiplet.[26]

For SrF_2:Eu^{3+} and BaF_2:Eu^{3+}, 77 K laser selective excitation measurements identified the dominant centers.[27,28] For SrF_2:Eu^{3+}, both C_{4v} and C_{3v} symmetry centers were observed together with an additional center of cubic O_h symmetry whose spectroscopy was also presented in a separate study including cubic centers for other alkaline-earth fluoride host lattices.[29] For BaF_2:Eu^{3+}, a single center of trigonal C_{3v} symmetry could be detected for concentrations less than 0.1 mol percent of the rare-earth dopant. The assignment of this center as trigonal is in disagreement with its adoption as being of C_{4v} symmetry by Silversmith and Macfarlane.[30] For the purposes of the latter work, a center of axial symmetry, either C_{4v} or C_{3v} could suffice.

In this paper, we present polarized laser selective excitation and Zeeman infrared-absorption measurements on CaF_2, SrF_2, and BaF_2 doped with Eu^{3+}. These follow earlier conference reports of upconverted fluorescence for these systems.[32] Detailed experimental and theoretical analyses of the axial-symmetry centers for these three hosts are presented. Polarized laser selective excitation is used to determine irreducible representations of the electronic energy levels while Zeeman-infrared absorption conclusively determines the site symmetries. Crystal- and magnetic-field analyses give an excellent account of the energy levels and of the measured magnetic splitting factors.

II. EXPERIMENT

The CaF_2, SrF_2, and BaF_2 crystals containing EuF_3 were grown by the Bridgman-Stockbarger method at the Univer-

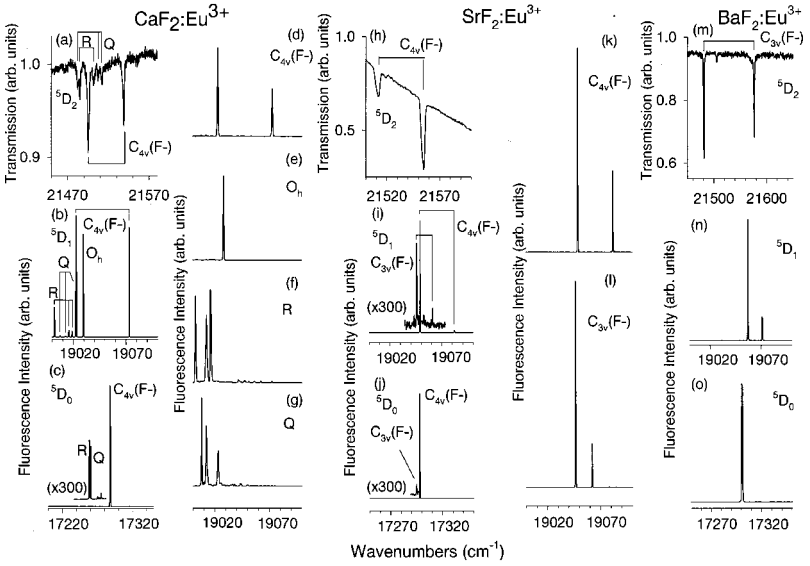

FIG. 1. (a), (h), and (m) 16 K $^5D_2$ optical-absorption spectra for CaF_2:0.15% Eu^{3+}, SrF_2:0.2% Eu^{3+}, and BaF_2:0.3% Eu^{3+}, respectively. (b), (i), and (n) 16 K laser excitation spectra for the $^5D_1$ multiplet in CaF_2:0.05% Eu^{3+}, SrF_2:0.05% Eu^{3+}, and BaF_2:0.05% Eu^{3+}, respectively. (c), (j), and (o) 16 K laser excitation spectra for the $^5D_0$ multiplet in CaF_2:0.05% Eu^{3+}, SrF_2:0.05% Eu^{3+}, and BaF_2:0.05% Eu^{3+}. Laser-selective excitation spectra (d) for the $C_{4v}(F^-)$ center (monitoring at 16 981 cm^{-1}), (e) for the O_h center (monitoring at 16 937 cm^{-1}), (f) for the R center (monitoring at 16 878 cm^{-1}) and (g) for the Q center (monitoring at 16 935 cm^{-1}) in CaF_2:0.05% Eu^{3+}. Laser-selective excitation spectra (k) for the $C_{4v}(F^-)$ center (monitoring at 16 974 cm^{-1}) and (l) for the $C_{3v}(F^-)$ center (monitoring at 16 442 cm^{-1}) in SrF_2:0.05% Eu^{3+}.

sity of Canterbury. In all cases, PbF_2 was added to the starting materials to scavenge for unintentional oxygen impurities. The starting materials were placed in a graphite crucible and lowered at 4 mmh^{-1} through the temperature gradient produced by the induction coils of a 38-kW rf furnace. Excellent optical quality samples were obtained and oriented crystals for polarization studies were cut from as grown boules, aligned using the (111) cleavage planes. Both the Eu^{3+} doped SrF_2 and BaF_2 crystals were completely clear, while the CaF_2 crystals were colored a light violet from the presence of Eu^{2+}. The divalent species is created through the reduction of some of the Eu^{3+} during the growth process.

The details of the experimental setup have been presented elsewhere and the reader is referred to Ref. 9, since identical equipment and techniques have been employed here.

III. OPTICAL SPECTROSCOPY OF Eu^{3+} IN CaF_2, SrF_2, AND BaF_2

A. Energy levels of Eu^{3+} ions in tetragonal and trigonal symmetry centers

The $4f^6$ configuration, appropriate for trivalent europium, consists of 3003 electronic states. Four multiplets of the ^5D term (with $J=0$, 1, 2, 3) have absorption transitions in the visible region. The ground multiplet is $^7F_0$ and fluorescence to all the ^7F_J multiplets could be observed. Typically, the optical transitions of Eu^{3+} are weak because of the spin selection rule. They could only be observed due to intermediate coupling effects that mix states of the same J but different L and S. Crystal-field J mixing of higher-lying states also occurs ($^7F_2$ is mixed into $^7F_0$, for example).

The standard notation of a letter plus a numerical subscript is used here for labeling the crystal-field levels of various LSJ multiplets. The ground multiplet is labeled Z, the $^7F_0$ ground state being Z_1, and the first excited multiplet $^7F_1$ labeled by Y. The single level of the $^5D_0$ multiplet is labeled by A, while those of $^5D_1$ are labeled as B_1 and B_2.

The Eu^{3+} energy levels have wave functions that transform as one of the irreducible representations (irreps) of the point group of the Eu^{3+} ions. For non-Kramers ions in C_{4v} symmetry centers, the energy levels transform as one of the nondegenerate irreps γ_1, γ_2, γ_3, γ_4 or the doubly degenerate γ_5 irrep, while for Eu^{3+} ions in centers of C_{3v} symmetry the wave-function symmetry can be labeled by the $\hat{\gamma}_1$, $\hat{\gamma}_2$ or $\hat{\gamma}_3$ irreps. The predicted polarization behavior of the levels for non-Kramers ions such as Eu^{3+} in C_{4v} and C_{3v} symmetry centers has been presented by Reeves *et al.*[2]

B. Absorption, laser selective excitation, and fluorescence spectra

Optical studies of Eu^{3+}-doped compounds are usually restricted to levels of the ^5D_J multiplets. For these weak spin-forbidden transitions, useful information is obtained by employing the high sensitivity and dynamic range of laser selective excitation.

Figure 1(a) shows absorption transitions to the $^5D_2$ multiplet of a 19.8 mm thick CaF_2:0.15% Eu^{3+} sample cooled to 16 K. These transitions have been assigned by comparison with the laser selective excitation spectra already presented in Ref. 4 and are assigned to a principal center of C_{4v} symmetry consisting of a single Eu^{3+}-F^- dipole and two cluster centers labeled R and Q.

The $^5D_1$ and $^5D_0$ laser excitation spectra are given in Figs. 1(b) and 1(c), respectively. Table I gives the $C_{4v}(F^-)$ center ^5D_J crystal states. The $^5D_1$ transitions show the same defect distribution as the $^7F_0 \rightarrow {}^5D_2$ transitions but as a consequence of their significant magnetic dipole moment, a single transition associated with a Eu^{3+} cubic-symmetry center is also observed. The relative intensity of the cubic-center transition [compared to the $C_{4v}(F^-)$ transitions] is strongly dependent on the Eu^{3+} concentration and is linked to the presence of anion excess clusters.[31] Figures 1(d)–1(g) show laser site selective excitation spectra of the $^5D_1$ multiplet for the $C_{4v}(F^-)$, O_h, R, and Q centers. The R and Q centers each give rise to three transitions. These centers have been previously assigned as dimer and trimer centers[23–25] and analogous Sm^{3+} ion centers have been observed for

TABLE I. Calculated and 16 K experimental energy levels (as measured in air, cm^{-1} ± 1) for the $C_{4v}(F^-)$ centers in $CaF_2:Eu^{3+}$ and $SrF_2:Eu^{3+}$. † indicates data from Ref. 27.

Multiplet	State and Symmetry	$CaF_2:Eu^{3+}$ Energy		$SrF_2:Eu^{3+}$ Energy	
		Calc	Expt	Calc	Expt
$^7F_0$	$Z_1\gamma_1$	0	0	2	0
$^7F_1$	$Y_1\gamma_5$	316	307	335	324
	$Y_1\gamma_2$	497	456	452	427
$^7F_2$	$X_1\gamma_4$	841	852	865	874
	$X_2\gamma_5$	971	971	961	968
	$X_3\gamma_3$	1134	1123	1154	1169
	$X_4\gamma_1$	1244	1261	1203	1221
$^7F_3$	$W_1\gamma_5$	1808	1814	1824	1835
	$W_2\gamma_4$	1828	1835	1849	1853
	$W_3\gamma_5$	1954	1953	1934(γ_2)	1936
	$W_4\gamma_2$	1977	1977	1938(γ_5)	1939
	$W_5\gamma_3$	2117	2130	2073	2084
$^7F_4$	$V_1\gamma_1$	2500	2510	2522	2531
	$V_2\gamma_5$	2764	2800	2773	2779
	$V_3\gamma_2$	2939	2947	2907	2921
	$V_4\gamma_5$	3003	3006	2979	2986
	$V_5\gamma_3$	3075	3089	3035	3051
	$V_6\gamma_4$	3106	3114	3078	3081
	$V_7\gamma_1$	3141	3156	3083	3114
$^7F_5$	$U_1\gamma_4$	3750	3747	3747	3748
	$U_2\gamma_5$	3832	3829	3819	3820
	$U_3\gamma_2$	3959	3970	3942	3960
	$U_4\gamma_3$	4031	4020	3985(γ_5)	3994
	$U_5\gamma_5$	4035	4035	4020(γ_3)	4021
	$U_6\gamma_5$	4113	4115	4067	4054
	$U_7\gamma_1$	4184	4183	4133	
	$U_8\gamma_2$	4185	4192	4134	4141
$^7F_6$	$T_1\gamma_4$	4885	4866	4911	4888
	$T_2\gamma_5$	4894	4873	4916	4892
	$T_3\gamma_1$	4902	4879	4917	4895
	$T_4\gamma_2$	5132	5150	5078	5055
	$T_5\gamma_5$	5159	5158	5117	5077
	$T_6\gamma_3$	5168		5142(γ_1)	5139
	$T_7\gamma_1$	5177	5167	5154(γ_5)	5140
	$T_8\gamma_5$	5216	5184	5151(γ_3)	5146
	$T_9\gamma_4$	5390		5285	
	$T_{10}\gamma_3$	5390		5285	
$^5D_0$	$A_1\gamma_1$	17 801	17 288	17 332	17 298
$^5D_1$	$B_1\gamma_5$	19 014	19 023	19 049	19 049
	$B_2\gamma_2$	19 086	19 073	19 095	19 082
$^5D_2$	$C_1\gamma_3$	21 452	21 455	21 482	21 480
	$C_2\gamma_1$	21 491	21 495	21 512	21 511
	$C_3\gamma_5$	21 519	21 537	21 542	21 554
	$C_4\gamma_4$	21 517		21 544	21 566†
$^5D_3$	$D_1\gamma_5$	24 337	24 335	24 373	24 373
	$D_2\gamma_3$	24 383	24 362	24 408	24 391
	$D_3\gamma_4$	24 358	24 371	24 390	24 401
	$D_4\gamma_2$	24 367	24 385	24 401	24 419
	$D_5\gamma_5$	24 409	24 397	24 426	24 436
Std Dev	σ		16		17

$CaF_2:Sm^{3+}$ and codoped variants.[9] The spectroscopy of these centers has been covered adequately, and thus, no further detail is given in this work.

The defect distribution for $SrF_2:Eu^{3+}$ is simpler. Absorption transitions to the $^5D_2$ multiplet for a 22.2-mm-thick sample doped to 0.2 molar percent are shown in Fig. 1(h). Two transitions are present, associated with a major center of C_{4v} symmetry. Laser selective excitation for the $^5D_1$ and $^5D_0$ multiplets were performed for SrF_2:0.05% Eu^{3+} samples [Figs. 1(i) and 1(j)]. Transitions of the $C_{4v}(F^-)$ center are observed together with weak $C_{3v}(F^-)$ center transitions at a factor of 300 times weaker. Figures 1(k) and 1(l) show laser site selective excitation spectra of the $^5D_1$ multiplet obtained for both centers. The $BaF_2:Eu^{3+}$ spectra show the presence of only one center of C_{3v} symmetry in Figs. 1(m)–1(o).

1. $C_{4v}(F^-)$ center in CaF_2:0.05% Eu^{3+} and SrF_2:0.05% Eu^{3+} crystals

The previous work on CaF_2 and SrF_2 doped with trivalent europium,[4,23–25,27] and the absorption and excitation spectra presented in this paper, indicate that the major center present has C_{4v} symmetry. In contrast to the previous studies that largely have concentrated on the defect distribution, these studies have constructed detailed energy-level schemes and determined irrep symmetries for the Eu^{3+} energy levels via polarized laser excitation experiments.

Figures 2 and 3 show polarized fluorescence spectra for the $C_{4v}(F^-)$ centers for [100] oriented CaF_2 and SrF_2 crystals doped with 0.05 mol percent Eu^{3+}. Both Figs. 2 and 3(a)–3(f) are fluorescence from the $^5D_0$ multiplet for Rhodamine 590 excitation. The $^7F_0 \rightarrow {}^5D_0$ pump transitions are electric-dipole allowed and thus the polarization geometry is $YX:YY$ as indicated in Figs. 2 and 3. As the $^5D_0$ multiplet consists of a single state transforming as a γ_1 singlet, only fluorescence transitions to states that are γ_1 orbital singlets or γ_5 doublets are electric-dipole allowed, while transitions terminating on states of γ_2 symmetry are magnetic-dipole allowed. Many polarization ratios obtained are significantly degraded from that predicted,[2] which is attributed to a mixed electric- and magnetic-dipole moment. This has been observed previously for the C_{4v} centers in CaF_2 and SrF_2 doped with Tb^{3+} (Ref. 5) and Sm^{3+} (Ref. 9).

Figures 2 and 3(g)–3(l) show polarized fluorescence from the $^5D_1$ multiplet excited using Coumarin 540 dye. The polarization dependence in the $ZX:ZY$ geometry confirms that the $^7F_0 \rightarrow {}^5D_1$ pump transitions are magnetic-dipole allowed. The observed fluorescence is complicated by overlapping fluorescence from $^5D_0$. For $CaF_2:Eu^{3+}$, some nonselectivity is caused by the overlap of a Q center transition with the C_{4v} center transition excited.

Figures 4 and 5 show polarized upconverted fluorescence for the C_{4v} centers in both crystals resonantly exciting the $^5D_0$ multiplet. These upconversion processes have been assigned as sequential absorption to high-lying Eu^{3+} states at around 34 600 cm^{-1}.[32] These decay nonradiatively to the ^5D_J multiplets from which optical fluorescence is observed.

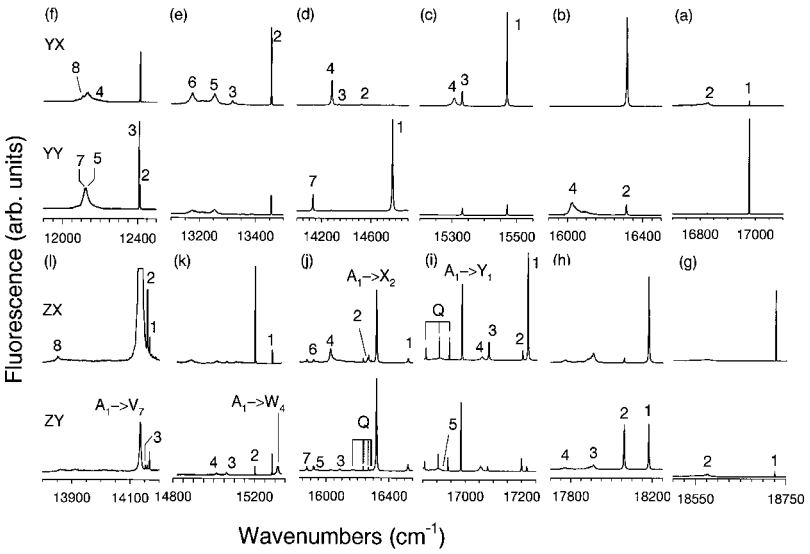

FIG. 2. 16 K polarized fluorescence spectra from $^5D_0$ to (a) $^7F_1$, (b) $^7F_2$, (c) $^7F_3$, (d) $^7F_4$, (e) $^7F_5$, and (f) $^7F_6$. From $^5D_1$ to (g) $^7F_1$, (h) $^7F_2$, (i) $^7F_3$, (j) $^7F_4$, (k) $^7F_5$, and (l) $^7F_6$ for the $C_{4v}(F^-)$ center in CaF_2:0.05% Eu^{3+}. The numerical notation used here denotes the terminating ($^7F_1$) state of the transition. Q denotes transitions of the Q cluster center.

The $^5D_3$ fluorescence places this upper multiplet at close to 24 370 cm^{-1}. Hamers, Wietfeldt, and Wright[4] placed it closer to 25 000 cm^{-1} for CaF_2:Eu^{3+} in disagreement with our results. Confidence in our assignments is obtained from consistency with other Eu^{3+} doped materials[33,34] and agreement with crystal-field calculations (Sec. V below). It is likely that Hamers, Wietfeldt, and Wright[4] were in fact exciting the $^5L_6$ multiplet. Table I gives the experimental crystal-field levels established for the $C_{4v}(F^-)$ centers in CaF_2:Eu^{3+} and SrF_2:Eu^{3+}.

2. $C_{3v}(F^-)$ center in SrF_2:0.05% Eu^{3+} and BaF_2:0.05% Eu^{3+} crystals

The laser selective excitation spectra revealed a minor center of C_{3v} symmetry in SrF_2:Eu^{3+} and the only center that is present in BaF_2:0.05% Eu^{3+} also has C_{3v} symmetry. Figures 6 and 7 show fluorescence for these two centers. The spectroscopic similarities of the spectra are striking and indicate that these two centers have the same charge compensation configuration. From the relative intensities of the $^7F_0 \rightarrow {}^5D_0$ transitions and the magnitude of the crystal-field splittings of the $J=1$ multiplets compared to the $C_{4v}(F^-)$ centers, it is apparent that these C_{3v} centers have only a weak axial distortion consistent with the remote placement of the charge compensating interstitial fluorine in the next-nearest-neighbor position along the [111] directions.

For the (111) oriented crystals, only weak polarization dependence is observed confirming the trigonal symmetry of the centers. As a consequence of the weak polarization dependence, the polarization ratios were typically hand measured and the spectra presented in Figs. 6 and 7 are unpolarized. As with the $C_{4v}(F^-)$ centers, these polarization ratios are degraded from those expected.[2] This is due to a mixed electric- or magnetic-dipole moment but may also be due to deviations from exact C_{3v} symmetry as has been reported previously for SrF_2:Er^{3+}.[10]

Upconversion fluorescence was observed for the $C_{3v}(F^-)$ center in BaF_2:Eu^{3+} and are shown in Figs. 7(m)–7(r). It

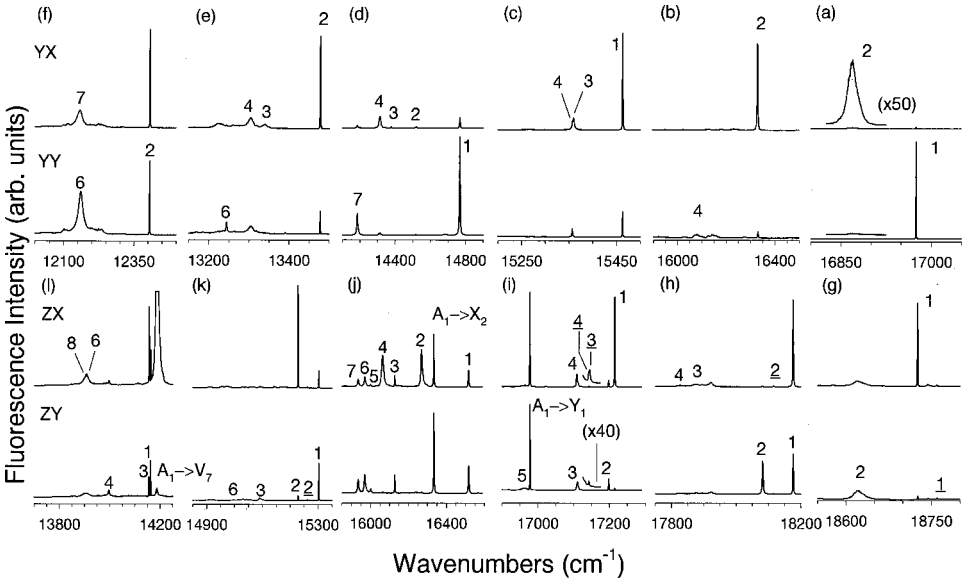

FIG. 3. 16 K polarized fluorescence spectra from $^5D_0$ to (a) $^7F_1$, (b) $^7F_2$, (c) $^7F_3$, (d) $^7F_4$, (e) $^7F_5$, and (f) $^7F_6$. From $^5D_1$ to (g) $^7F_1$, (h) $^7F_2$, (i) $^7F_3$, (j) $^7F_4$, (k) $^7F_5$, and (l) $^7F_6$ for the $C_{4v}(F^-)$ center in SrF_2:0.05% Eu^{3+}. The numerical notation used here denotes the terminating ($^7F_1$) state of the transition. An underline is used to denote transitions orginating from the 1st excited upper state.

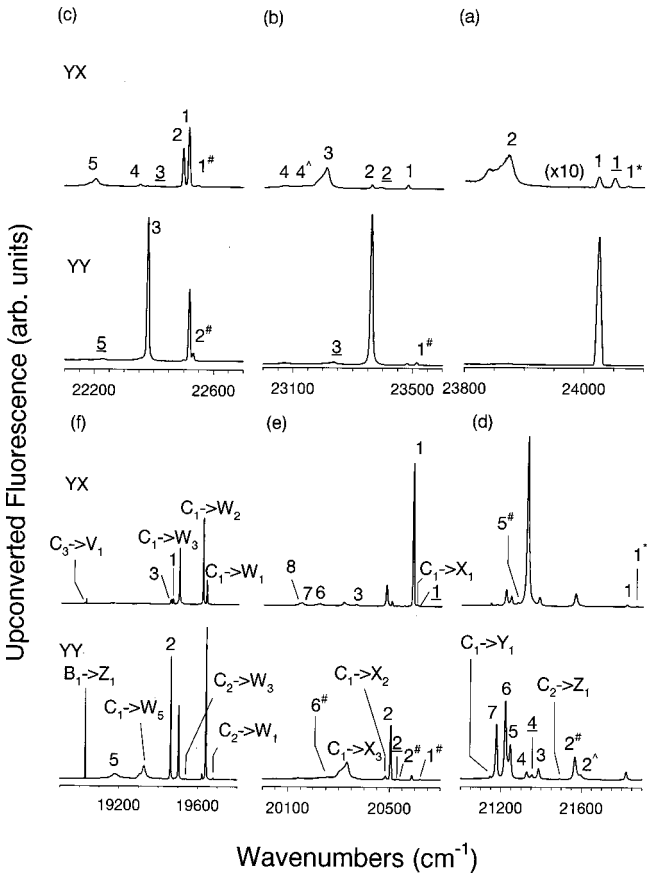

FIG. 4. 16 K polarized upconversion fluorescence spectra from $^5D_3$ to (a) $^7F_1$, (b) $^7F_2$, (c) $^7F_3$, (d) $^7F_4$, (e) $^7F_5$, and (f) $^7F_6$ for the $C_{4v}(F^-)$ center in CaF_2:0.05% Eu^{3+}. The numerical notation used here denotes the terminating ($^7F_1$), state of the transition. An underline is used to denote transition orginating from the 1st excited upper state, superscript # from the 2nd excited state, superscript * from the 3rd excited state, and superscript from the 4th excited state. Transitions emanating from $^5D_2$ and $^5D_1$ are labeled separately.

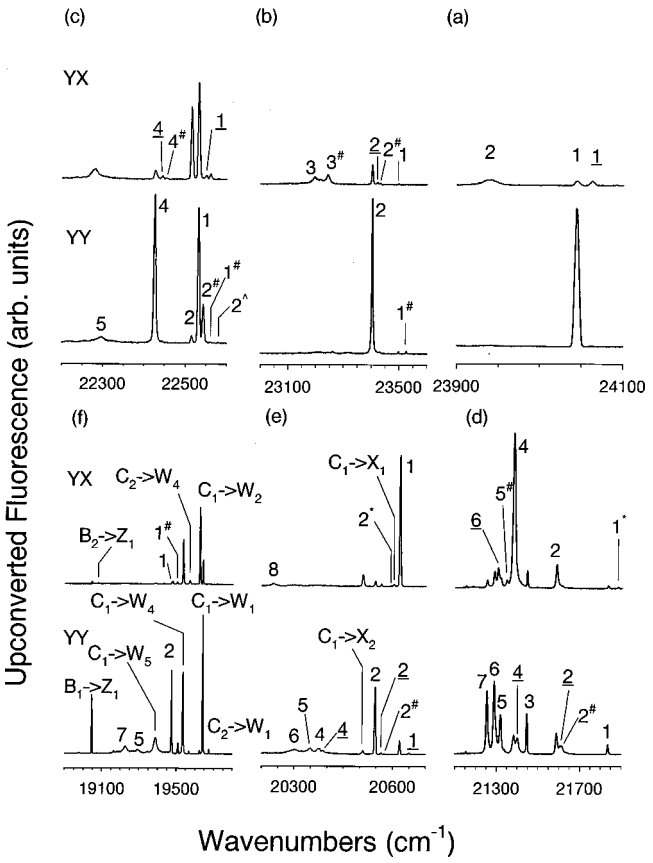

FIG. 5. 16 K polarized upconversion fluorescence spectra from $^5D_3$ to (a) $^7F_1$, (b) $^7F_2$, (c) $^7F_3$, (d) $^7F_4$, (e) $^7F_5$, and (f) $^7F_6$ for the $C_{4v}(F^-)$ center in SrF_2:0.05% Eu^{3+}. The numerical notation used here denotes the terminating ($^7F_1$), state of the transition. An underline is used to denote transitions orginating from the 1st excited upper state, superscript # from the 2nd excited state, superscript * from the 3rd excited state, and superscript ^ from the 4th excited state. Transitions emanating from $^5D_2$ and $^5D_1$ are labeled separately.

was not possible to observe upconversion for the SrF_2:Eu^{3+} $C_{3v}(F^-)$ center since the transitions available for excitation were considerably weaker than those of the BaF_2 center. The $C_{3v}(F^-)$ center energy levels for both SrF_2:Eu^{3+} and BaF_2:Eu^{3+} are presented in Table II. A noticeable feature of the fluorescence recorded for the $C_{3v}(F^-)$ centers in both materials is the prominence of the one-phonon sidebands coupled to the Eu^{3+} electronic states. The observed phonon-displacement frequencies correspond to peaks in the respective host-lattice phonon density of states. A sharp feature in the BaF_2:Eu^{3+}, $^5D_0 \rightarrow {}^7F_2$ spectrum at 16 431 cm^{-1} cannot be assigned to emission from $^5D_0$ and is tentatively ascribed to upconverted emission from the $^5D_2$ multiplet due to its close match with the expected $C_1 \rightarrow T_4$ transition energy.

3. Fluorescent lifetimes

The 16 K fluorescence lifetimes for the $^5D_0$, $^5D_1$ and $^5D_2$ multiplets have been measured for the $C_{4v}(F^-)$ centers in CaF_2:Eu^{3+} and SrF_2:Eu^{3+} and for the $C_{3v}(F^-)$ center in BaF_2:Eu^{3+} and are given in Table III. The lifetimes for the $^5D_0$ multiplets are relatively long at around 13 milliseconds. This is a consequence of the radiative nature of the decay of the $^5D_0$ multiplet, itself a direct result of the large energy gap to the nearest ^7F multiplet at close to 12 000 cm^{-1}. Trends across the alkaline-earth series show an increase in lifetime with increasing ionic radius of the alkaline-earth cation. This is entirely consistent with the proposed charge compensation configurations for these centers as the interstitial F^- ion (responsible for the predominantly electric-dipole character of the emitted radiation) becomes progressively distant as we proceed through the host cations. The measured $^5D_1$ and $^5D_2$ lifetimes follow the differing phonon cutoff energies for the three hosts, modified by the exact composition of the electronic wave functions.

IV. INFRARED AND ZEEMAN INFRARED ABSORPTION

A. CaF_2:Eu^{3+} and SrF_2:Eu^{3+}

Transitions from $^7F_0$ to the levels of the ^7F multiplets can be observed by infrared absorption. Multiphonon host-lattice

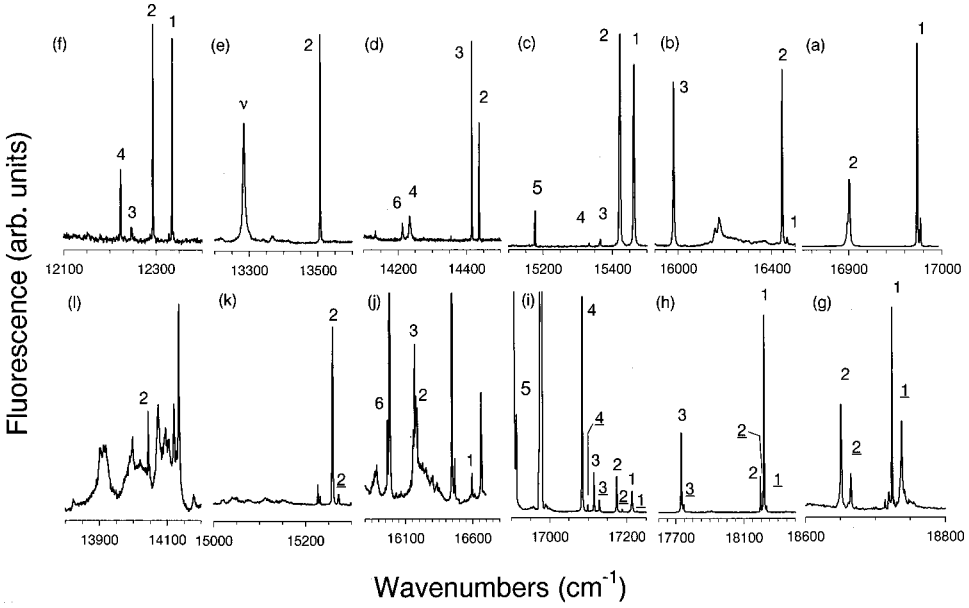

FIG. 6. 16 K unpolarized fluorescence spectra for $^5D_0$ to (a) $^7F_1$, (b) $^7F_2$, (c) $^7F_3$, (d) $^7F_4$, (e) $^7F_5$, and (f) $^7F_6$. From $^5D_1$ to (g) $^7F_1$, (h) $^7F_2$, (i) $^7F_3$, (j) $^7F_4$, (k) $^7F_5$, and (l) $^7F_6$ for the $C_{3v}(F^-)$ center in SrF_2:0.05% Eu^{3+}. The v notation is used to indicate a strong vibronic peak. All other symbols are as defined previously.

absorption limits these observable transitions to the $^7F_2$ to $^7F_6$ multiplets. In addition, the electric-dipole selection rule allows observation to only those multiplets satisfying $\Delta J = 2, 4, 6$ for transitions from the $^7F_0$ state. Figure 8 shows 16 K infrared-absorption transitions to the $^7F_2$, $^7F_3$, $^7F_4$, and $^7F_6$ multiplets for 25-mm-thick CaF_2:0.05% Eu^{3+} and a 29-mm-thick SrF_2:0.05% Eu^{3+} crystal. The observation of transitions to the $^7F_3$ multiplet indicate the admixture of states of different J through crystal-field J mixing. The infrared transitions are assigned from comparison with laser selective excitation presented in Sec. III. The observed spectra for CaF_2:Eu^{3+} are rendered more complicated than those of SrF_2:Eu^{3+} by the presence of R and Q center cluster transitions whose levels are known from previous studies.[4,35] Transitions to the $^7F_4$ multiplet for both CaF_2 and SrF_2 show a transition asociated with cubic centers. While $\Delta J = 4$ transitions have no magnetic-dipole moment it is possible that this can occur through crystal-field J mixing with the $^7F_1$ multiplet. Weak C_{3v} center transitions also appear for SrF_2:Eu^{3+} [inset in Fig. 7(g)].

4.2 K Zeeman infrared-absorption measurements were performed on the $C_{4v}(F^-)$ centers for (111) oriented crystals. For the magnetic field directed along the (111) crystallographic axis, all C_{4v} centers are magnetically equivalent, and the Eu^{3+} site symmetry is reduced to C_1. With a nondegenerate ground state, a doublet splitting that corresponds to the lifting of the twofold degeneracy of the excited-state orbital doublet is expected. The derived $C_{4v}(F^-)$ center magnetic splitting factors are presented in Table IV.

Particularly interesting Zeeman splittings are observed for the $T_1\gamma_4$, $T_2\gamma_5$, and $T_3\gamma_1$ states. Figure 9 shows the infrared-absorption spectra for these states as a function of applied-magnetic field along the [111] direction for both CaF_2:Eu^{3+} and SrF_2:Eu^{3+}. The observed Zeeman patterns are markedly nonlinear as a consequence of second-order Zeeman interactions that mix in components of the doublet with the two

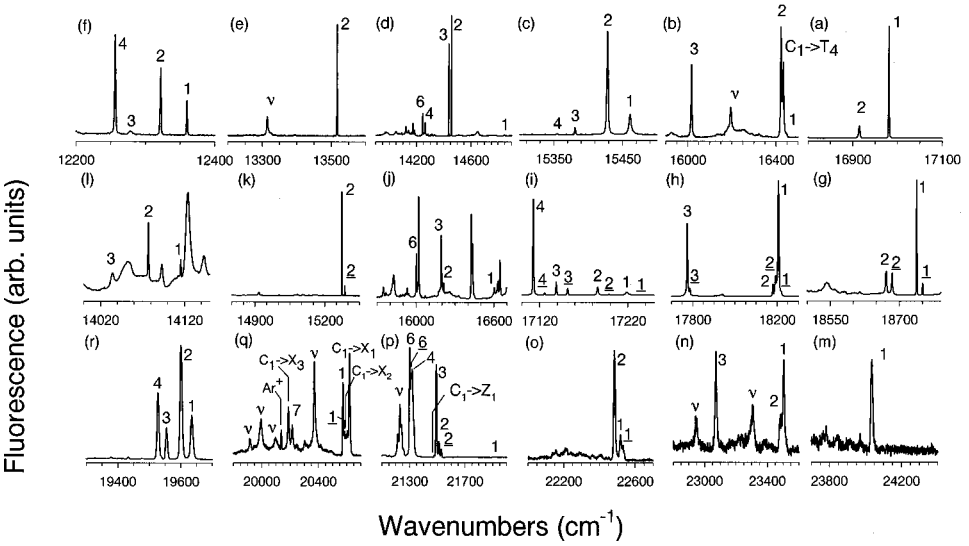

FIG. 7. 16 K unpolarized fluorescence spectra for $^5D_0$ to (a) $^7F_1$, (b) $^7F_2$, (c) $^7F_3$, (d) $^7F_4$, (e) $^7F_5$, and (f) $^7F_6$. From $^5D_1$ to (g) $^7F_1$, (h) $^7F_2$, (i) $^7F_3$, (j) $^7F_4$, (k) $^7F_5$, and (l) $^7F_6$ Upconverted fluorescence spectra from $^5D_3$ to (m) $^7F_1$, (n) $^7F_2$, (o) $^7F_3$, (p) $^7F_4$, and (q) $^7F_5$; (r) from $^5D_2$ to $^7F_3$ for the $C_{3v}(F^-)$ center in BaF_2:0.05% Eu^{3+}. The v notation is used to indicate a strong vibronic peak. All other symbols are as defined previously.

TABLE II. Calculated and 16 K experimental energy levels (as measured in air, cm^{-1} ± 1) for the $C_{3v}(F^-)$ centers in SrF_2:Eu^{3+} and BaF_2:Eu^{3+}. † indicates data from Refs. 27 and 28.

Multiplet	State and Symmetry	SrF_2:Eu^{3+} Energy		BaF_2:Eu^{3+} Energy	
		Calc	Expt	Calc	Expt
$^7F_0$	$Z_1\hat{\gamma}_1$	−1	0	0	0
$^7F_1$	$Y_1\hat{\gamma}_3$	334	322	343	325
	$Y_2\hat{\gamma}_2$	406	396	398	391
$^7F_2$	$X_1\hat{\gamma}_3$	834	831	856	852
	$X_2\hat{\gamma}_1$	856	853	868	883
	$X_3\hat{\gamma}_3$	1281	1316	1254	1288
$^7F_8$	$W_1\hat{\gamma}_2$	1835	1836	1842	1842
	$W_2\hat{\gamma}_3$	1877	1875	1868	1875
	$W_3\hat{\gamma}_1$	1947	1934	1927	1922
	$W_4\hat{\gamma}_3$	1965	1967	1948	1948
	$W_5\hat{\gamma}_2$	2126	2121	2100	-
$^7F_4$	$V_1\hat{\gamma}_1$	2445	2454	2462	2458
	$V_2\hat{\gamma}_2$	2846	2860	2832	2848
	$V_3\hat{\gamma}_3$	2846	2881	2837	2867
	$V_4\hat{\gamma}_3$	3084	3063	3058	3040
	$V_5\hat{\gamma}_1$	3095		3068	
	$V_6\hat{\gamma}_3$	3103	3084	3069	3059
$^7F_5$	$U_1\hat{\gamma}_3$	3785		3782	
	$U_2\hat{\gamma}_1$	3800	3791	3788	3787
	$U_3\hat{\gamma}_2$	3951		3937	
	$U_4\hat{\gamma}_3$	3955		3942	
	$U_5\hat{\gamma}_2$	4131		4111	
	$U_6\hat{\gamma}_3$	4141		4112	
	$U_7\hat{\gamma}_3$	4189		4151	4146
$^7F_6$	$T_1\hat{\gamma}_1$	4957	4962	4948	4943
	$T_2\hat{\gamma}_3$	5002	5003	4990	4982
	$T_3\hat{\gamma}_3$	5064	5049	5041	5024
	$T_4\hat{\gamma}_2$	5072	5073	5048	5047
	$T_5\hat{\gamma}_1$	5088		5052	
	$T_6\hat{\gamma}_1$	5247		5212	
	$T_7\hat{\gamma}_2$	5248		5215	
	$T_8\hat{\gamma}_3$	5254		5224	
	$T_9\hat{\gamma}_3$	5263		5228	
$^5D_0$	$A_1\hat{\gamma}_1$	17 306	17 295	17 329	17 303
$^5D_1$	$B_1\hat{\gamma}_3$	19 034	19 046	19 055	19 057
	$B_2\hat{\gamma}_2$	19 055	19 061	19 071	19 071
$^5D_2$	$C_1\hat{\gamma}_3$	21 460	21 454†	21 480	21 482
	$C_2\hat{\gamma}_3$	21 529		21 543	21 565†
	$C_3\hat{\gamma}_2$	21 535		21 550	21 571†
$^5D_3$	$D_1\hat{\gamma}_3$			24 372	24 362
	$D_2\hat{\gamma}_1$			24 385	24 376
	$D_3\hat{\gamma}_2$			24 400	
	$D_4\hat{\gamma}_3$			24 409	
	$D_5\hat{\gamma}_2$			24 415	
Std Dev	σ		17		17

singlets states. The Zeeman operator (J_z) transforms as a γ_2 and can connect the three crystal-field states. The mixing of the $T_2\gamma_5$ with the $T_1\gamma_4$ state also has the effect of lending the transition moment of the doublet to the singlet, thereby creating nonvanishing matrix elements for the electric-dipole operator between the $^7F_0(Z_1\gamma_1)$ and $^7F_6(T_1\gamma_4)$ states. This is observable in Fig. 9 by the appearance of the transition to T_1 at fields higher than 1 Tesla.

TABLE III. 16 K fluorescent lifetimes (in milliseconds $\pm 5\%$) for the $^5D_2$, $^5D_1$, and $^5D_0$ multiplets of the $C_{4v}(F^-)$ centers in CaF_2:Eu^{3+} and SrF_2:Eu^{3+}, and the $C_{3v}(F^-)$ center in BaF_2:Eu^{3+}.

Crystal	Site Symmetry	Lifetime		
		$^5D_0$	$^5D_1$	$^5D_2$
CaF_2	C_{4v}	11.8	3.6	1.6
SrF_2	C_{4v}	13.4	5.9	5.4
BaF_2	C_{3v}	14.6	10.3	6.3

B. BaF_2:Eu^{3+}

Figure 10 shows 4.2 K infrared-absorption spectra for a 11.1-mm-thick BaF_2:0.1% Eu^{3+} crystal. Transitions to both the $^7F_4$ and $^7F_6$ multiplets could be observed. The absence of transitions to the $^7F_2$ and $^7F_3$ multiplets is a result of the small axial field experienced by the Eu^{3+} ions in the $C_{3v}(F^-)$ centers. A weak cubic-center transition is observed to the $^7F_4$ multiplet at 2884.2 cm^{-1}.

Figure 10 also shows Zeeman infrared-absorption spectra for magnetic fields applied along the [100] and [111] directions in order to conclusively determine the symmetry of the Eu^{3+} ion center. Of all the observed transitions, those to the $^7F_4(V_3\gamma_3)$ and $^7F_6(T_2\gamma_3)$ states at 2869.2 and 4984.7 cm^{-1}, respectively, have been assigned as doublets from the laser selective excitation measurements and only these states show a Zeeman splitting.

For the magnetic field along a (111) direction, there are two magnetically inequivalent trigonal centers giving rise to Zeeman patterns of four lines. One of the four trigonal center orientations is along the magnetic-field B, while the other three are equally inclined to the magnetic field and experi-

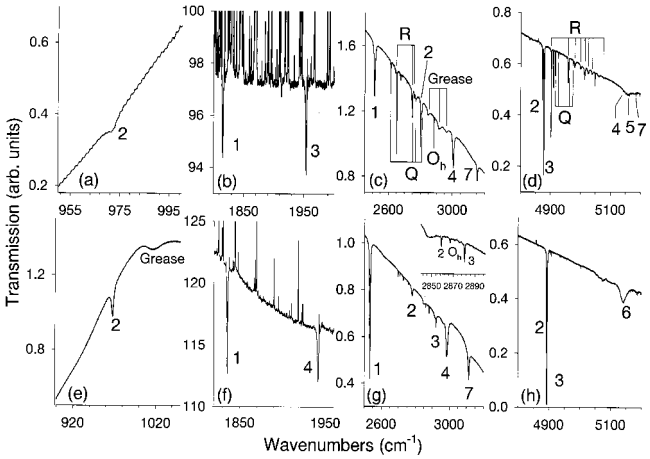

FIG. 8. 16 K infrared absorption spectra for (a) $^7F_2$, (b) $^7F_3$, (c) $^7F_4$, and (d) $^7F_6$ in CaF_2:0.05% Eu^{3+}, (e) $^7F_2$, (f) $^7F_3$, (g) $^7F_4$, and (h) $^7F_6$ in SrF_2:0.05% Eu^{3+}. The sharp upward spikes in (b) and (f) result from the subtraction of a water vapor background.

TABLE IV. [111] Zeeman splitting factors (calculated and experimental (± 0.2)) for the $C_{4v}(F^-)$ centers in CaF_2:Eu^{3+} and SrF_2:Eu^{3+} determined from Zeeman infrared absorption.

		Magnetic Splitting Factors			
		CaF_2		SrF_2	
State	Field (Tesla)	Calc	Expt	Calc	Expt
X_1	4	2.0		1.99	2.0
W_1	4	0.71		0.44	0.6
W_3	3	2.6	2.2	2.70	2.3 ± 0.3 (W_4)
T_2	4	0.21	~0.3	1.08	1.0

ence a field component of $(1/3)B$ along their symmetry axis, giving one third the Zeeman splitting for their absorption lines. The combined pattern is four equally spaced lines with a 1:3:3:1 intensity pattern, and the splitting of the outside pair arising from trigonal centers along the field. The measured magnetic splitting factors are $s_{\|}=1.03$ and $s_{\text{inclined}}=0.35$ for the V_3 upper state, and $s_{\|}=3.0$ and $s_{\text{inclined}}=1.6$ for the T_2 upper state. Unlike the V_3 doublet, the Zeeman splittings of the T_2 state do not have even line separations due to magnetic-field admixtures between the crystal-field wave functions that yield a nonzero perpendicular Zeeman splitting factor.

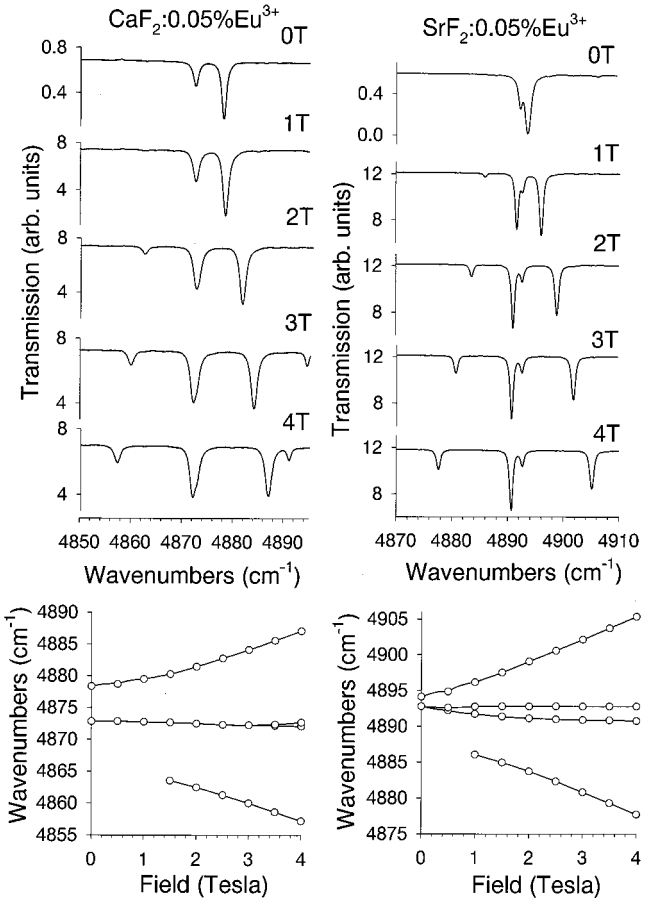

FIG. 9. 4.2 K, Zeeman splittings as a function of applied magnetic field for the $^7F_6$, $T_1\gamma_4$, $T_2\gamma_5$, and $T_3\gamma_1$ states of CaF_2:0.05% Eu^{3+} and SrF_2:0.05% Eu^{3+}.

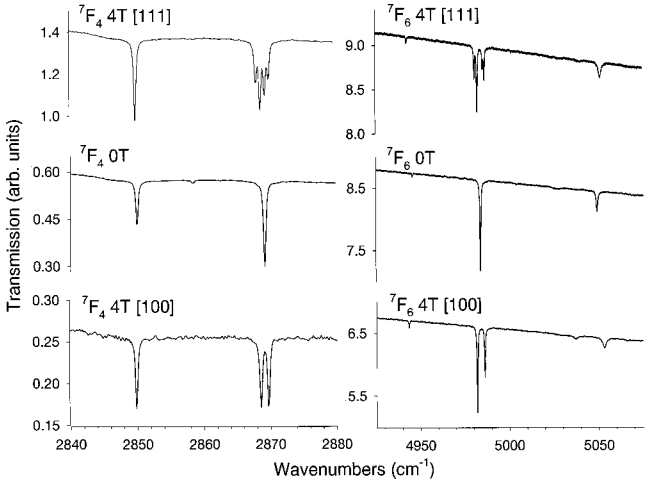

FIG. 10. 4.2 K, zero field and four Tesla Zeeman spectra for [111] and [100] applied magnetic fields for the $^7F_4$ and $^7F_6$ multiplets of BaF_2:0.1% Eu^{3+}.

For the magnetic field along a (100) direction, all trigonal centers are equally inclined to the magnetic field at an angle of $\cos^{-1}(1/\sqrt{3})$ yielding a single Zeeman split line pair. The measured splitting factors are $s_{(100)}=0.6$ and $s_{(100)}=2.3$ for the V_3 and T_2 states, respectively. These (111) and (100) Zeeman measurements conclusively confirm the trigonal symmetry of the principal center for BaF_2:Eu^{3+}.

A particular feature of the Zeeman spectrum is the displacement in the field of the 5049.7 cm^{-1} singlet level. In the (111) $4T$ field it has moved 2.5 cm^{-1} and in the (100) $4T$ field it has moved 4.0 cm^{-1} to higher energy. This is caused by nonlinear Zeeman interactions between this singlet level and a nearby γ_2 singlet.

Extremely weak splittings could also be observed for the SrF_2:Eu^{3+} $C_{3v}(F^-)$ center, $^7F_4(V_3\gamma_3)$ transition at 2881.2 cm^{-1} for a (111) magnetic-field direction. These yield splitting factors of $s_{\|}=1.22$ and $s_{(111)}=0.39$ that are similar to those measured for BaF_2:Eu^{3+}.

V. CRYSTAL- AND MAGNETIC-FIELD ANALYSIS OF THE $C_{4v}(F^-)$ AND $C_{3v}(F^-)$ CENTERS

Crystal-field analyses have been performed using the *f*-shell empirical programs of Dr. Mike Reid. These assist in the determination of irrep symmetry and are used to interpret Zeeman splitting factors. The combined free-ion and crystal-field Hamiltonian matrices for the $4f^6$ configuration were diagonalized for a truncated set of $4f^6$ basis states of the lowest 400 electronic states (approximately the lowest 40 multiplets) as a realistic approximation for the entire $4f^6$ configuration. The free-ion Hamiltonian is parametrized as follows:[36]

$$H_{fi}=\sum_{k=2,4,6}F^k f_k+\sum_i \zeta_i\cdot s_i+\alpha L(L+1)+\beta G(G_2)$$
$$+\gamma G(R_\gamma)+\sum_{h=0,2,4}M^h m_h+\sum_{k=0,2,4,6}P^k p_k$$
$$+\sum_{i=2,3,4,6,7,8}T^i t_i .$$

The major terms in this Hamiltonian are the electrostatic and spin-orbit interactions represented by the parameters F^k and ζ. The residual terms represent interactions of significantly smaller magnitude that play a role in accounting for the energy level structure of the $4f^6$ configuration. These are the configuration interaction (α,β,γ), spin-spin and spin-other-obit interactions represented by the parameters M^h, the two-body electrostatically correlated magnetic interactions, with parameters P^k, and the three-particle configuration interactions, T^i. Only the electrostatic and spin-orbit parameters were varied in the fitting procedure, while the remaining parameters are held constant at the values given in Ref. 36. As only levels of the ^5D and ^{7}F terms have been experimentally determined, the F^4 and F^6 parameters were constrained to the ratios $F^4/F^2=0.71$ and $F^6/F^2=0.51$ as obtained for LaF_3:Eu^{3+} in Ref. 36, via a new parameter F^{tot}.

The crystal-field Hamiltonians appropriate for C_{4v} and C_{3v} symmetries, in terms of Racah spherical tensor $C_q^{(k)}$ (Ref. 37) have:

$$\begin{aligned}H_{\mathrm{tet}}=&B_A^2C_0^{(2)}+B_A^4\{C_0^{(4)}-\sqrt{\tfrac{7}{10}}\,[C_4^{(4)}+C_{-4}^{(4)}]\}\\&+B_A^6\{C_0^{(6)}+\sqrt{\tfrac{1}{14}}\,[C_4^{(6)}+C_{-4}^{(6)}]\}\\&+B_C^4\{C_0^{(4)}+\sqrt{\tfrac{5}{14}}\,[C_4^{(4)}+C_{-4}^{(4)}]\}\\&+B_C^6\{C_0^6+\sqrt{\tfrac{7}{2}}\,[C_4^{(6)}+C_{-4}^{(6)}]\}.\end{aligned}$$

$$\begin{aligned}H_{\mathrm{trig}}=&B_A^2C_0^{(2)}+B_A^4\{C_0^{(4)}-\tfrac{1}{2}\sqrt{\tfrac{7}{10}}\,[C_3^{(4)}-C_{-3}^{(4)}]\}\\&+B_A^6\{\sqrt{\tfrac{11}{42}}\,[C_3^{(6)}-C_{-3}^{(6)}]+\sqrt{\tfrac{5}{21}}\,[C_6^{(6)}+C_{-6}^{(6)}]\}\\&+B_A^6\{C_0^{(6)}+\tfrac{4}{7}\sqrt{\tfrac{10}{21}}\,[C_3^{(6)}-C_{-3}^{(6)}]-\tfrac{4}{7}\sqrt{\tfrac{11}{21}}\\&\times[C_6^{(6)}+C_{-6}^{(6)}]\}+B_C^4\{C_0^{(4)}+\sqrt{\tfrac{10}{7}}\,[C_3^{(4)}-C_{-3}^{(4)}]\}\\&+B_C^6\{C_0^{(6)}-\sqrt{\tfrac{35}{96}}\,[C_3^{(6)}-C_{-3}^{(6)}]\\&+\tfrac{1}{8}\sqrt{\tfrac{77}{3}}\,[C_6^{(6)}+C_{-6}^{(6)}]\},\end{aligned}$$

where the tensor combinations are the invariant scalars under the point group-symmetry reduction chains $SO_3\rightarrow O\rightarrow D_4\rightarrow C_4$ and $SO_3\rightarrow O\rightarrow D_3\rightarrow C_3$, respectively. The parameters of these Hamiltonians are grouped into $B_C^{(k)}$ terms which form a cubic symmetry Hamiltonian and $B_A^{(k)}$ terms that represent the noncubic components as appropriate for C_{4v} or C_{3v} symmetries.

Crystal-field fits to the 45 and 46 energy levels determined for the $C_{4v}(F^-)$ centers in CaF_2:Eu^{3+} and SrF_2:Eu^{3+}, and the 24 and 29 energy levels determined for the $C_{3v}(F^-)$ centers in SrF_2:Eu^{3+} and BaF_2:Eu^{3+} were performed with the results from laser selective excitation (see Tables I and II). For the C_{4v} symmetry centers, seven free parameters were employed in the fits to obtain standard deviations of 16 and 17 cm^{-1} for CaF_2:Eu^{3+} and SrF_2:Eu^{3+}, respectively. The resulting crystal-field parameters, shown in Table V, are consistent with those previously reported for other rare-earth ions.[1,3,5,6,8,9,38,39] Table IV gives the calculated (111) magnetic splitting factors for the $C_{4v}(F^-)$ centers that well match those measured from Zeeman infrared absorption.

TABLE V. Optimized free-ion and crystal-field parameters for the $C_{4v}(F^-)$ and $C_{3v}(F^-)$ centers in CaF_2:Eu^{3+}, SrF_2:Eu^{3+}, and BaF_2:Eu^{3+}. Those in square brackets were not varied but were held at the values in Ref. 36.

	CaF_2:Eu^{3+}	SrF_2:Eu^{3+}		BaF_2:Eu^{3+}
Parameter	C_{4v}	C_{4v}	C_{3v}	C_{3v}
F_{tot}	83 233	83 378	83 206	83 316
α	[20.16]	[20.16]	[20.16]	[20.16]
β	[−566.9]	[−566.9]	[−566.9]	[−566.9]
γ	[1500]	[1500]	[1500]	[1500]
T^2	[300]	[300]	[300]	[300]
T^3	[40]	[40]	[40]	[40]
T^4	[60]	[60]	[60]	[60]
T^6	[−300]	[−300]	[−300]	[−300]
T^7	[370]	[370]	[370]	[370]
T^8	[320]	[320]	[320]	[320]
M_{tot}	[2.1]	[2.1]	[2.1]	[2.1]
M_{tot}	[360]	[360]	[360]	[360]
ζ	1327	1326	1327	1325
B_A^2	714	458	217	165
B_A^4	446	372	106	161
B_A^6	551	482	−47	−40
$B_{\bar{A}}^6$			−193	−107
B_C^4	−1211	−1182	1227	1124
B_C^6	665	561	1091	1031
n	45	46	25	29
σ	16	17	17	17

The $C_{3v}(F^-)$ center crystal-field fits yield standard deviations of 17 cm^{-1} for both SrF_2:Eu^{3+} and BaF_2:Eu^{3+} (see Table IV). The resulting crystal-field parameters give good agreement with those of Ref. 10 for the so-called *J* center in SrF_2:Eu^{3+} and compare well with those obtained for the $C_{3v}(F^-)$ center in BaF_2:Er^{3+}.[40] Both the SrF_2 and BaF_2 centers have only weak axial distortions from the placement of a nearest-neighbor F^- interstitial along the (111) direction, making these centers quite close to cubic in their spectroscopic properties.

VI. CONCLUSIONS

Optical absorption and laser selective excitation and fluorescence has enabled the construction of energy-level schemes for the four major crystal-field centers in CaF_2, SrF_2, and BaF_2 crystals doped with trivalent europium. From polarized laser selective excitation and Zeeman infrared absorption, the Eu^{3+} centers comprise the well-established $C_{4v}(F^-)$ and $C_{3v}(F^-)$ centers. The latter is only weakly present for SrF_2:Eu^{3+} and is the only center found for BaF_2:Eu^{3+}. The unambiguous determination of a C_{3v} symmetry center in BaF_2:Eu^{3+} resolves conflicts in the literature where the center has been assigned to have either C_{4v} or C_{3v} symmetries.

The Zeeman infrared-absorption measurements for the $^7F_6$ multiplet reveal notably nonlinear Zeeman patterns from the mixing between excited-state singlets and a doublet for both CaF_2:Eu^{3+} and SrF_2:Eu^{3+}. These mixing effects are also observable in BaF_2:Eu^{3+} as a nonzero perpendicular Zeeman interaction for the excited state doublets of the Eu^{3+} ion.

Crystal-field analyses give good account of the $C_{4v}(F^-)$ and $C_{3v}(F^-)$ center energy levels with excellent agreement between the crystal-field parameters obtained in this study and those of previous workers. The inclusion of the Zeeman operator in the combined free-ion and crystal-field Hamiltonian yields magnetic splitting factors that accurately account for the measured Zeeman splittings.

ACKNOWLEDGMENTS

This research has been supported by the University of Canterbury and the New Zealand Lotteries Board. The authors would like to thank Dr. Mike F. Reid of the University of Canterbury for supplying his crystal-field fitting programs and Dr. Glynn D. Jones for many informative discussions. Technical assistance has been provided by R. A. Ritchie, W. Smith, and R. Culley.

*Current address and corresponding author. Dr. Jon-Paul R. Wells, FELIX Free-Electron Laser Facility, FOM-Institute for Plasma-physics ''Rijnhuizen,'' Edisonbaan 14, P.O. Box 1207, 3430 BE, Nieuwegein, The Netherlands; Email address: wells@rijnh.nl; FAX: +31-30-6031204.

[1] C. A. Freeth and G. D. Jones, J. Phys. Chem. **15**, 6833 (1982).
[2] R. J. Reeves, G. D. Jones, and R. W. G. Syme, Phys. Rev. B **46**, 5939 (1992); B. M. Tissue and J. C. Wright, *ibid.* **36**, 9781 (1987).
[3] T. P. J. Han, G. D. Jones, and R. W. G. Syme, Phys. Rev. B **47**, 14 706 (1993).
[4] R. J. Hamers, J. R. Wietfeldt, and J. C. Wright, J. Chem. Phys. **77**, 683 (1982).
[5] G. D. Jones and K. M. Murdoch, J. Lumin. **60&61**, 131 (1993); K. M. Murdoch, G. D. Jones, and R. W. G. Syme, Phys. Rev. B **56**, 1254 (1997).
[6] M. Mujaji, G. D. Jones, and R. W. G. Syme, Phys. Rev. B **46**, 14 398 (1992); M. B. Seelbinder and J. C. Wright, *ibid.* **20**, 4308 (1979).
[7] N. J. Cockroft, D. Thompson, G. D. Jones, and R. W. G. Syme, J. Chem. Phys. **86**, 521 (1987); D. R. Tallant and J. C. Wright, *ibid.* **63**, 2074 (1975).
[8] N. M. Strickland and G. D. Jones, Phys. Rev. B **56**, 10 916 (1997).
[9] J.-P. R. Wells and R. J. Reeves, Phys. Rev. B **61**, 13 593 (2000).
[10] N. J. Cockroft, G. D. Jones, and R. W. G. Syme, J. Chem. Phys. **92**, 2166 (1990); M. D. Kurz and J. C. Wright, J. Lumin. **15**, 169 (1977).
[11] R. L. Cone, P. C. Hansen, M. J. M. Leask, and B. M. Wanklyn, J. Phys.: Condens. Matter **5**, 573 (1993).
[12] A. Meijerink and J. C. Wright, J. Lumin. **53**, 116 (1992).
[13] P. Porcher and P. Caro, J. Chem. Phys. **65(1)**, 89 (1976).
[14] P. Porcher and P. Caro, J. Chem. Phys. **68(9)**, 4176 (1978).
[15] P. Porcher and P. Caro, J. Chem. Phys. **68(9)**, 4183 (1978).
[16] W. Ryba-Romanowski, S. Golab, W. A. Pisarski, G. Dominiak-Dzik, M. Berkowski, and A. Pajaczkowska, J. Phys. Chem. Solids **58(4)**, 639 (1997).
[17] R. L. Cone, P. C. Hansen, and M. J. M. Leask, J. Opt. Soc. Am. B **9(5)**, 779 (1992).
[18] A. J. Silversmith and N. B. Manson, Phys. Rev. B **34(7)**, 4854 (1986).
[19] G. K. Liu, R. Cao, and J. V. Beitz, J. Alloys Compd. **225**, 45 (1995).
[20] G. P. Flinn, K. W. Jang, J. Ganem, M. L. Jones, R. S. Meltzer, and R. M. Macfarlane, Phys. Rev. B **49**, 5821 (1994).
[21] Yu K. Voronko, A. A. Kaminskii, and V. V. Osiko, Sov. Phys. JETP **22**, 501 (1966).
[22] B. P. Zakharchenya and I. B. Rusanov, Sov. Phys. Solid State **8**, 31 (1966).
[23] K. M. Cirillo-Penn and J. C. Wright, Phys. Rev. B **41**, 10 799 (1990).
[24] K. M. Cirillo-Penn and J. C. Wright, J. Lumin. **48&49**, 505 (1991).
[25] K. M. Cirillo-Penn and J. C. Wright, Radiat. Eff. Defects Solids **119–121**, 231 (1991).
[26] J.-P. R. Wells, G. D. Jones, and R. J. Reeves, J. Lumin. **72–74**, 977 (1997).
[27] J. P. Jouart, C. Bisseux, G. Mary, and M. Egee, J. Phys. C **18**, 1539 (1985).
[28] J. P. Jouart, C. Bisseux, and G. Mary, J. Lumin. **37**, 159 (1987).
[29] J. P. Jouart, M. Bouffard, G. Klein, and G. Mary, J. Lumin. **50**, 273 (1991).
[30] A. J. Silversmith and R. M. Macfarlane, Phys. Rev. B **45**, 5811 (1992).
[31] P. P. Yaney, D. M. Schaeffer, and J. L. Wolf, Phys. Rev. B **11**, 2460 (1975).
[32] J.-P. R. Wells and R. J. Reeves, J. Lumin. **66&67**, 219 (1996).
[33] M. Dejneka, E. Snitzer, and R. E. Riman, J. Lumin. **65**, 227 (1995).
[34] R. Reisfeld and L. Boehm, J. Solid State Chem. **4**, 417 (1972).
[35] J.-P. R. Wells, Ph.D. thesis, University of Canterbury (1997).
[36] W. T. Carnall, G. L. Goodman, K. Rajnak, and R. S. Rana, J. Chem. Phys. **90**(7), 3443 (1989).
[37] B. G. Wybourne, *Spectroscopic Properties of Rare-Earths* (Interscience, New York, 1965).
[38] J.-P. R. Wells, G. D. Jones, and R. J. Reeves, Phys. Rev. B **60**(2), 851 (1999).
[39] C. A. Freeth, G. D. Jones, and R. W. G. Syme, J. Phys. C **15**, 5667 (1982).
[40] J.-P. R. Wells, T. Dean, and R. J. Reeves, J. Lumin. (submitted).